Performance Analysis of Aerial RIS Auxiliary mmWave Mobile Communications With UAV Fluctuation

Baiping Xiong, *Graduate Student Member, IEEE*, Zaichen Zhang, *Senior Member, IEEE*, Cunhua Pan, *Senior Member, IEEE*, and Jiangzhou Wang, *Fellow, IEEE*

***Abstract*—Reconfigurable intelligent surface (RIS) has emerged as a key enabler to boost the performance in the upcoming wireless networks in a spectral/cost/energy-efficient manner. In contrast to terrestrial RISs coated on facades of buildings, aerial RISs benefit from flexible mobility and full-angle reflection by mounting the RISs on aerial platforms such as unmanned aerial vehicles (UAVs). However, the aerial platforms are sensitive to inevitable fluctuation, causing performance variations. In this letter, we develop a novel channel model for UAV-mounted RIS auxiliary millimeter wave (mmWave) mobile systems in the presence of UAV attitude fluctuation. Based on the proposed channel model, the closed-form expression for the signal-to-noise ratio (SNR) in terms of UAV attitude fluctuation is derived. The impact of fluctuation on the array receiving aperture and the maximum SNR is investigated. The *filtering effect* on maximum SNR brought by fluctuation is revealed, arising for the requirement of UAV attitude detection. Numerical results are provided to verify the accuracy of our derived results.**

***Index Terms*—Aerial RIS, mmWave mobile communications, performance analysis, UAV fluctuation.**

I. Introduction

MILLIMETER wave (mmWave) wireless communications with adaptive directional beamforming are considered promising to support high data rate and low latency services for future mobile networks such as vehicular communications by leveraging the abundant bandwidth as well as directional transmission [1]. However, the terrestrial mmWave vehicular networks are vulnerable to blockage, causing severe performance deterioration.

For the purpose of contributing favourable propagation environments for transmission, reconfigurable intelligent surface (RIS) has been witnessed a spectral/cost/energy-efficient solution [2]. Different from terrestrial RISs with limited coverage, mounting RISs on aerial platforms such as unmanned aerial vehicles (UAVs), which is referred to as aerial RISs, can provide on-demand dynamic deployment and panoramic full-angle coverage [3]. Compared with the mmWave full-duplex UAV relay, aerial RIS brings no noise and is cost- and energy-efficient due to the lack of radio frequency chains as well as signal processing capability. Specifically, the authors in [4] considered the application of aerial RIS for jamming mitigation in secure communications by jointly optimizing the aerial RIS deployment and reflection phase. The authors in [5] proposed to deploy UAV-mounted RIS to provide wireless services for maritime users in the easy-blocking offshore areas. The weighted sum rate maximization of a multi-UAV-carried RISs assisted system was considered in [6], which was verified to be superior to the terrestrial counterpart via simulations. In [7], the throughput of a massive multiple-input multiple-output (MIMO) network that explores the advantages of UAV and RIS was investigated, where the results showed that the proposed scheme achieves high throughput with low complexity.

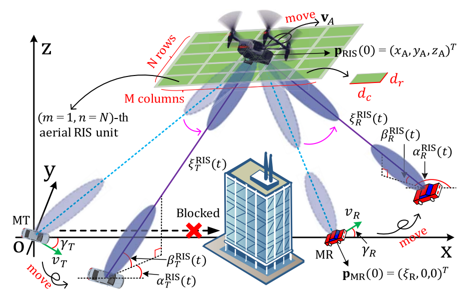

Fig. 1. Illustration of the proposed aerial RIS assisted mmWave mobile communications with UAV fluctuation.

The aerial platforms are generally sensitive to inevitable fluctuations, resulting in navigation and attitude variations and therefore performance variations [8]. This, however, has not been revealed in the existing literature on aerial RIS-assisted communications. To this end, we propose a novel channel model for aerial RIS auxiliary mmWave mobile communications taking the UAV attitude fluctuation into account. Based on the proposed model, we derive the closed-form expression for the mapping relationship between the signal-to-noise ratio (SNR) and the attitude fluctuation. The impact of fluctuation on the aerial RIS receiving aperture, which contributes to the squared-power gain of the aerial RIS [9], is also investigated. We reveal the *filtering effect* on the maximum SNR brought by fluctuation and investigate the impacts of different fluctuation models on the system performance.

Notation: Throughout this letter, non-boldface, boldface lowercase, and boldface uppercase letters denote scalar, vector, and matrix, respectively; $|\cdot|$, $(\cdot)^T$, and $\langle\cdot,\cdot\rangle$ stand for absolute value, transpose, and vector dot product, respectively; $\mathbb{E}(\cdot)$ and $\|\cdot\|$ take the expectation and ℓ_2-norm, respectively.

Manuscript received 4 January 2024; accepted 7 February 2024. Date of publication 12 February 2024; date of current version 11 April 2024. This work was supported by NSFC under Project 61960206005; in part by the Jiangsu Key Research and Development Program under Project BE2023011-2; in part by the Fundamental Research Funds for the Central Universities under Grant 2242022k60001; and in part by the Research Fund of National Mobile Communications Research Laboratory under Grant 2024A04. The associate editor coordinating the review of this article and approving it for publication was G. L. A. Aruma Baduge. *(Corresponding author: Zaichen Zhang.)*

Baiping Xiong, Zaichen Zhang, and Cunhua Pan are with the National Mobile Communications Research Laboratory, Southeast University, Nanjing 210096, China (e-mail: xiongbp@seu.edu.cn; zczhang@seu.edu.cn; cpan@seu.edu.cn).

Jiangzhou Wang is with the School of Engineering, University of Kent, CT2 7NT Canterbury, U.K. (e-mail: j.z.wang@kent.ac.uk).

Digital Object Identifier 10.1109/LWC.2024.3364831

TABLE I
SUMMARY OF KEY PARAMETER DEFINITIONS

$\xi_T^{\mathrm{RIS}}(t)$, $\xi_R^{\mathrm{RIS}}(t)$	distances between MT/MR and aerial RIS
$\alpha_T^{\mathrm{RIS}}(t)$, $\beta_T^{\mathrm{RIS}}(t)$	AAoD and EAoD from MT to aerial RIS
$\alpha_R^{\mathrm{RIS}}(t)$, $\beta_R^{\mathrm{RIS}}(t)$	AAoA and EAoA from aerial RIS to MR
M, N	column/row numbers of aerial RIS (top view)
d_c, d_r	size of RIS unit in column/row direction (top view)
ψ_T, ϕ_T	azimuth/elevation orientation angle of MT ULA
M_T, δ_T	antenna number and spacing of MT ULA
ψ_R, ϕ_R	azimuth/elevation orientation angle of MR ULA
M_R, δ_R	antenna number and spacing of MR ULA
v_T, γ_T	motion speed and direction of MT
v_R, γ_R	motion speed and direction of MR
v_A, γ_A, η_A	motion speed/azimuth/elevation direction of aerial RIS

II. SYSTEM MODEL

As illustrated in Fig. 1, let us consider a MIMO mmWave mobile communication system with blocked LoS path between the ground transceivers, where an UAV-mounted RIS is deployed to assist the signal transmission by establishing a virtual LoS link between the ground mobile transceivers. The definition of the key model parameters are summarized in Table I. The ground mobile transmitter (MT) is in motion with velocity vector $\mathbf{v}_T = v_T[\cos\gamma_T, \sin\gamma_T, 0]^T$ and is equipped with an omnidirectional uniform linear array (ULA). The distance vector from the center of the MT ULA to the p-th $(p = 1, 2, \ldots, M_T)$ antenna is denoted by $\mathbf{d}_p = \frac{M_T-2p+1}{2}\delta_T\,[\cos\phi_T\cos\psi_T, \cos\phi_T\sin\psi_T, \sin\phi_T]^T$. Similarly, at the ground mobile receiver (MR), we have $\mathbf{v}_R = v_R[\cos\gamma_R, \sin\gamma_R, 0]^T$ and $\mathbf{d}_q = \frac{M_R-2q+1}{2}\delta_R[\cos\phi_R\cos\psi_R, \cos\phi_R\sin\psi_R, \sin\phi_R]^T$. The aerial RIS, with velocity vector $\mathbf{v}_A = v_A[\cos\eta_A\cos\gamma_A, \cos\eta_A\sin\gamma_A, \sin\eta_A]^T$, is fabricated with MN reflecting units in a uniform planar array (UPA) structure. Following the global coordinate system (GCS) definition in [10], the locations of the central points of the MT ULA, aerial RIS, and MR ULA at time instant $t = 0$, i.e., time instant at which we begin to observe the channel, are represented as $\mathbf{p}_{\mathrm{MT}}(0) = (0, 0, 0)^T$, $\mathbf{p}_{\mathrm{RIS}}(0) = (x_{\mathrm{A}}, y_{\mathrm{A}}, z_{\mathrm{A}})^T$, and $\mathbf{p}_{\mathrm{MR}}(0) = (\xi_R, 0, 0)^T$, respectively. After a time interval of t, their locations turn to be $\mathbf{p}_{\mathrm{MT}}(t) = \mathbf{p}_{\mathrm{MT}}(0) + \mathbf{v}_T t$, $\mathbf{p}_{\mathrm{RIS}}(t) = \mathbf{p}_{\mathrm{RIS}}(0) + \mathbf{v}_A t$, and $\mathbf{p}_{\mathrm{MR}}(t) = \mathbf{p}_{\mathrm{MR}}(0) + \mathbf{v}_R t$, respectively.

In the proposed aerial RIS auxiliary mmWave mobile communication system, let s be the transmitted symbol with power $\mathbb{E}\{ss^*\} = P_T$, $n(t)$ denote the zero-mean complex Gaussian noise with variance σ^2, and $\mathbf{H}_{\mathrm{TR}}(t, f) \in \mathbb{C}^{M_R\times M_T}$ be the frequency domain channel matrix between the mobile transceivers, respectively. Then, the corresponding received signal model could be described by [2]

$$y(t) = \mathbf{f}_{\mathrm{MR}}^T(t)\mathbf{H}_{\mathrm{TR}}(t, f)\ \mathbf{f}_{\mathrm{MT}}(t)s + n(t), \tag{1}$$

where $\mathbf{f}_{\mathrm{MR}}(t) \in \mathbb{C}^{M_R\times 1}$ and $\mathbf{f}_{\mathrm{MT}}(t) \in \mathbb{C}^{M_T\times 1}$ represent the MR combining and MT beamforming vectors, respectively. In the following, we firstly present the UAV attitude fluctuation model adopted in this letter, and then derive the complex channel matrix $\mathbf{H}_{\mathrm{TR}}(t, f)$ in the presence of UAV fluctuation.

A. UAV Attitude Fluctuation Modeling

In the local coordinate system (LCS) x′-y′-z′ on the aerial RIS plane, as defined in Fig. 2 (a), the unit vector along the negative direction of the z′-axis, also named the unit normal

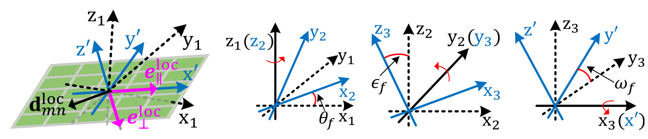

(a) unit vectors on aerial RIS (b) yaw angle (c) pitch angle (d) roll angle

Fig. 2. Definition of aerial RIS fluctuation angles. The axes in $\mathrm{x_1}$-$\mathrm{y_1}$-$\mathrm{z_1}$ are parallel to those in x-y-z of Fig. 1, the x′-y′-z′ is defined on aerial RIS plane.

vector of the aerial RIS, is expressed as

$$\boldsymbol{e}_\perp^{\mathrm{loc}} = [0 \quad 0 \quad -1]^T, \tag{2}$$

and the unit vector along the positive direction of the x′-axis, i.e., the unit direction vector of the aerial RIS, is expressed as

$$\boldsymbol{e}_\parallel^{\mathrm{loc}} = [1 \quad 0 \quad 0]^T. \tag{3}$$

Moreover, the distance vector from the center of the aerial RIS to the (m, n)-th ($m = 1, 2, \ldots, M$; $n = 1, 2, \ldots, N$) aerial RIS unit in the LCS x′-y′-z′ is expressed as

$$\begin{aligned}\mathbf{d}_{mn}^{\mathrm{loc}} &= [k_m d_c \ -k_n d_r \ 0]^T \\ &= \left[\tfrac{2m-M-1}{2} d_c \ -\tfrac{2n-N-1}{2} d_r \ 0\right]^T.\end{aligned} \tag{4}$$

In this letter, we aim at establishing a mapping relationship between the amount of attitude fluctuation and the system performance, and hence adopt the Euler angles representation of the attitude fluctuation angles as described in [8]. Then, the transformation from the LCS $\mathrm{x_1}$-$\mathrm{y_1}$-$\mathrm{z_1}$ to the LCS x′-y′-z′ can be uniquely characterized by three successive fluctuations, i.e., yawing, pitching, and rolling, whose sequence cannot be changed due to the specific significance of the Euler angles [11]. As shown in Figs. 2 (b)-(d), we use θ_f to denote the yaw angle of the aerial RIS resulting from a fluctuation of θ_f around the $\mathrm{z_1}$-axis, use ϵ_f to denote the pitch angle of the aerial RIS resulting from a fluctuation of ϵ_f around the $\mathrm{y_2}$-axis, and use ω_f to denote the roll angle of the aerial RIS resulting from a fluctuation of ω_f around the $\mathrm{x_3}$-axis, respectively. In this case, the LCS x′-y′-z′ can be obtained by firstly translating the GCS x-y-z from point (0, 0, 0) to point $(x_{\mathrm{A}}, y_{\mathrm{A}}, z_{\mathrm{A}})$, and then fluctuating it by yaw angle θ_f, pitch angle ϵ_f, and roll angle ω_f in the aforementioned three directions, successively. Consequently, the transformation of the representation of arbitrary vector from the LCS x′-y′-z′ to the GCS x-y-z or vice versa could be realized by multiplying the corresponding rotation matrix. Specifically, the representation of the unit normal vector $\boldsymbol{e}_\perp^{\mathrm{loc}}$ in the GCS x-y-z, denoted by $\boldsymbol{e}_\perp$, could be expressed as [8]

$$\begin{aligned}\boldsymbol{e}_\perp &= \mathbf{R}_{\mathrm{yaw}}(\theta_f)\mathbf{R}_{\mathrm{pitch}}(\epsilon_f)\mathbf{R}_{\mathrm{roll}}(\omega_f)\boldsymbol{e}_\perp^{\mathrm{loc}} \\ &= \begin{bmatrix}\cos\theta_f & -\sin\theta_f & 0\\ \sin\theta_f & \cos\theta_f & 0\\ 0 & 0 & 1\end{bmatrix} \times \begin{bmatrix}\cos\epsilon_f & 0 & \sin\epsilon_f\\ 0 & 1 & 0\\ -\sin\epsilon_f & 0 & \cos\epsilon_f\end{bmatrix} \\ &\quad \times \begin{bmatrix}1 & 0 & 0\\ 0 & \cos\omega_f & -\sin\omega_f\\ 0 & \sin\omega_f & \cos\omega_f\end{bmatrix} \times \begin{bmatrix}0\\ 0\\ -1\end{bmatrix} \\ &= \begin{bmatrix}-\cos\theta_f\sin\epsilon_f\cos\omega_f - \sin\theta_f\sin\omega_f\\ -\sin\theta_f\sin\epsilon_f\cos\omega_f + \cos\theta_f\sin\omega_f\\ -\cos\epsilon_f\cos\omega_f\end{bmatrix},\end{aligned} \tag{5}$$

where $\mathbf{R}_{\text{yaw}}(\theta_f)$, $\mathbf{R}_{\text{pitch}}(\epsilon_f)$, and $\mathbf{R}_{\text{roll}}(\omega_f)$ are the rotation matrices corresponding to the yaw, pitch, and roll fluctuations of the aerial RIS, respectively.

Similarly, the representation of the unit direction vector $\boldsymbol{e}_{\|}^{\text{loc}}$ in the GCS x-y-z, that is, $\boldsymbol{e}_{\|}$, could be obtained by

$$\boldsymbol{e}_{\|} = \mathbf{R}_{\text{yaw}}(\theta_f)\mathbf{R}_{\text{pitch}}(\epsilon_f)\mathbf{R}_{\text{roll}}(\omega_f)\boldsymbol{e}_{\|}^{\text{loc}} = \begin{bmatrix} \cos\theta_f \cos\epsilon_f \\ \sin\theta_f \cos\epsilon_f \\ -\sin\epsilon_f \end{bmatrix}, \tag{6}$$

and the representation of the distance vector $\mathbf{d}_{mn}^{\text{loc}}$ in the GCS x-y-z, denoted by $\mathbf{d}_{mn}$, is expressed in (7), as shown at the bottom of the page. The results through (5)–(7) show that the aerial RIS attitude fluctuation will cause the variations of the model parameters, imposing non-negligible effect on the channel response and therefore on the system performance.

B. Channel Response of the Proposed Channel Model

The frequency domain channel matrix is interpreted as $\mathbf{H}_{\text{TR}}(t,f) = [h_{pq}(t,f)]_{M_R \times M_T}$, where $h_{pq}(t,f)$ denotes the channel coefficient between the p-th ($p = 1,2,\ldots,M_T$) transmit antenna and the q-th ($q = 1,2,\ldots,M_R$) receive antenna. Since the aerial RIS is in the air with considerable altitude, we assume that the LoS link dominates the mmWave directional propagation between the aerial RIS and the ground transceivers [12]. Then, the $h_{pq}(t,f)$ can be expressed as

$$\begin{aligned} h_{pq}(t,f) = \sqrt{\frac{\Omega_{\text{RIS}}(t)}{\Upsilon_{pq}(t)}} \sum_{m=1}^{M}\sum_{n=1}^{N} \chi_{mn}(t) e^{j\varphi_{mn}(t)} \\ \times e^{-j\frac{2\pi}{\lambda}\left(\xi_{mn}^{p}(t)+\xi_{mn}^{q}(t)\right)} \times e^{j2\pi f \tau_{\text{RIS}}(t)} \\ \times e^{j\frac{2\pi}{\lambda}\langle(\mathbf{v}_T-\mathbf{v}_A)t,\, \boldsymbol{e}_T^{\text{RIS}}(t)\rangle} e^{j\frac{2\pi}{\lambda}\langle(\mathbf{v}_R-\mathbf{v}_A)t,\, \boldsymbol{e}_R^{\text{RIS}}(t)\rangle}, \end{aligned} \tag{8}$$

where λ is the wavelength, $\Upsilon_{pq}(t)$ is the normalized factor, $\Omega_{\text{RIS}}(t)$ stands for the path power gain including the path loss, $\xi_{mn}^{p}(t) = \|\mathbf{p}_{\text{RIS}}(t) - \mathbf{p}_{\text{MT}}(t) + \mathbf{d}_{mn} - \mathbf{d}_p\|$ and $\xi_{mn}^{q}(t) = \|\mathbf{p}_{\text{RIS}}(t) - \mathbf{p}_{\text{MR}}(t) + \mathbf{d}_{mn} - \mathbf{d}_q\|$ are the signal traveling distances from the p-th transmit antenna and the q-th receive antenna to the (m, n)-th aerial RIS unit, respectively. The $\tau_{\text{RIS}}(t) = (\xi_T^{\text{RIS}}(t) + \xi_R^{\text{RIS}}(t))/c$ is the path delay from the MT to the MR via the aerial RIS, $\boldsymbol{e}_T^{\text{RIS}}(t)$ and $\boldsymbol{e}_R^{\text{RIS}}(t)$ represent the unit directional vectors from the MT and the MR to the aerial RIS, respectively, which are expressed as [3]

$$\boldsymbol{e}_{T/R}^{\text{RIS}}(t) = \begin{bmatrix} \cos\beta_{T/R}^{\text{RIS}}(t)\cos\alpha_{T/R}^{\text{RIS}}(t) \\ \cos\beta_{T/R}^{\text{RIS}}(t)\sin\alpha_{T/R}^{\text{RIS}}(t) \\ \sin\beta_{T/R}^{\text{RIS}}(t) \end{bmatrix}. \tag{9}$$

To gain more insightful results, we adopt the following approximations for $\xi_{mn}^{p}(t)$ based on the Taylor series expansion in the far-field case [8]

$$\begin{aligned} \xi_{mn}^{p}(t) &\approx \|\mathbf{p}_{\text{RIS}}(t) - \mathbf{p}_{\text{MT}}(t)\| + (\mathbf{d}_{mn} - \mathbf{d}_p)^T \frac{\mathbf{p}_{\text{RIS}}(t) - \mathbf{p}_{\text{MT}}(t)}{\|\mathbf{p}_{\text{RIS}}(t) - \mathbf{p}_{\text{MT}}(t)\|} \\ &= \xi_T^{\text{RIS}}(t) + (\mathbf{d}_{mn} - \mathbf{d}_p)^T \boldsymbol{e}_T^{\text{RIS}}(t), \end{aligned} \tag{10}$$

$$\frac{1}{\xi_{mn}^{p}(t)} \approx \frac{1}{\|\mathbf{p}_{\text{RIS}} - \mathbf{p}_{\text{MT}}(t)\|} = \frac{1}{\xi_T^{\text{RIS}}(t)}, \tag{11}$$

where $\boldsymbol{e}_T^{\text{RIS}}(t) = \frac{\mathbf{p}_{\text{RIS}}(t) - \mathbf{p}_{\text{MT}}(t)}{\|\mathbf{p}_{\text{RIS}}(t) - \mathbf{p}_{\text{MT}}(t)\|}$. Similarly, for $\xi_{mn}^{q}(t)$, we have

$$\xi_{mn}^{q}(t) \approx \xi_R^{\text{RIS}}(t) + \left(\mathbf{d}_{mn} - \mathbf{d}_q\right)^T \boldsymbol{e}_R^{\text{RIS}}(t), \tag{12}$$

$$\frac{1}{\xi_{mn}^{q}(t)} \approx \frac{1}{\xi_R^{\text{RIS}}(t)}. \tag{13}$$

With the approximations through (10)–(13), $\Upsilon_{pq}(t)$ is approximated by

$$\begin{aligned} \Upsilon_{pq}(t) \approx \mathbb{E}\Big\{\Big| \sum_{m=1}^{M}\sum_{n=1}^{N} \chi_{mn}(t) \\ \times e^{j\left(\varphi_{mn}(t) - \frac{2\pi}{\lambda}\left(\mathbf{d}_{mn}^T \boldsymbol{e}_T^{\text{RIS}}(t) + \mathbf{d}_{mn}^T \boldsymbol{e}_R^{\text{RIS}}(t)\right)\right)}\Big|^2\Big\}, \end{aligned} \tag{14}$$

and subsequently the $\Omega_{\text{RIS}}(t)$ can be approximated by [2]

$$\Omega_{\text{RIS}}(t) \approx \frac{\lambda^2 d_c d_r \cos\beta_{\text{in}}^{\text{RIS}}(t)}{(4\pi)^3\left(\xi_T^{\text{RIS}}(t)\xi_R^{\text{RIS}}(t)\right)^2} \times \Upsilon_{pq}(t), \tag{15}$$

where $\beta_{\text{in}}^{\text{RIS}}(t)$ is the normal incident angle of the signals from the MT to the aerial RIS, and it can be represented as [13]

$$\begin{aligned} \cos\beta_{\text{in}}^{\text{RIS}}(t) &= \frac{\boldsymbol{e}_{\perp}^T\left(-\boldsymbol{e}_T^{\text{RIS}}(t)\right)}{\|\boldsymbol{e}_{\perp}\|\|-\boldsymbol{e}_T^{\text{RIS}}(t)\|} \\ &= \sin\epsilon_f \cos\omega_f \cos\beta_T^{\text{RIS}}(t)\cos\left(\alpha_T^{\text{RIS}}(t) - \theta_f\right) \\ &\quad - \sin\omega_f \cos\beta_T^{\text{RIS}}(t)\sin\left(\alpha_T^{\text{RIS}}(t) - \theta_f\right) \\ &\quad + \cos\epsilon_f \cos\omega_f \sin\beta_T^{\text{RIS}}(t). \end{aligned} \tag{16}$$

It shows that the attitude fluctuation of the aerial RIS will affect the aerial RIS receiving aperture through affecting the normal incident angle $\beta_{\text{in}}^{\text{RIS}}(t)$, and hence affects the channel gain as well as the system performance.

Note that the derivations of other model parameters including $\{\xi_T^{\text{RIS}}(t), \xi_R^{\text{RIS}}(t), \alpha_T^{\text{RIS}}(t), \beta_T^{\text{RIS}}(t), \alpha_R^{\text{RIS}}(t), \beta_R^{\text{RIS}}(t)\}$ follow the similar procedure discussed in [2], [13] by exploiting the geometric relationship among MT, aerial RIS, and MR, as well as the moving speeds/directions/times of the terminals and will not be presented in this letter due to the space limitation

III. Performance Analysis With UAV Fluctuation

The signal-to-noise ratio (SNR) of the proposed aerial RIS auxiliary communication system in the presence of UAV fluctuation can be written as

$$\eta(t) = \frac{P_T|\mathbf{f}_{\text{MR}}^T(t)\mathbf{H}_{\text{TR}}(t,f)\ \mathbf{f}_{\text{MT}}(t)|^2}{\sigma^2}. \tag{17}$$

We assume that the channel state information (CSI) is available, then the maximal-ratio combining strategy [14], i.e., $\mathbf{f}_{\text{MT}}(t) = \frac{1}{\sqrt{M_T}}[e^{-j\frac{2\pi}{\lambda}\mathbf{d}_{p=1}^T \boldsymbol{e}_T^{\text{RIS}}(t)}, \ldots, e^{-j\frac{2\pi}{\lambda}\mathbf{d}_{p=M_T}^T \boldsymbol{e}_T^{\text{RIS}}(t)}]^T$ and $\mathbf{f}_{\text{MR}}(t) = \frac{1}{\sqrt{M_R}}[e^{-j\frac{2\pi}{\lambda}\mathbf{d}_{q=1}^T \boldsymbol{e}_R^{\text{RIS}}(t)},$

$$\mathbf{d}_{mn} = \mathbf{R}_{\text{yaw}}(\theta_f)\mathbf{R}_{\text{pitch}}(\epsilon_f)\mathbf{R}_{\text{roll}}(\omega_f)\mathbf{d}_{mn}^{\text{loc}} = \begin{bmatrix} \cos\theta_f\cos\epsilon_f k_m d_c - \left(\cos\theta_f\sin\epsilon_f\sin\omega_f - \sin\theta_f\cos\omega_f\right)k_n d_r \\ \sin\theta_f\cos\epsilon_f k_m d_c - \left(\sin\theta_f\sin\epsilon_f\sin\omega_f + \cos\theta_f\cos\omega_f\right)k_n d_r \\ -\sin\epsilon_f k_m d_c - \cos\epsilon_f\sin\omega_f k_n d_r \end{bmatrix}. \tag{7}$$

$\ldots, e^{-j\frac{2\pi}{\lambda}\mathbf{d}_{q=M_R}^T \boldsymbol{e}_R^{\mathrm{RIS}}(t)}]^T$, gives the following maximum SNR

$$\eta(t) = \frac{M_T M_R P_T \Omega_{\mathrm{RIS}}(t)}{\sigma^2}. \tag{18}$$

We further assume that the aerial RIS reflection coefficient can be programmed on demand without loss. The fluctuation of the UAV, however, is unavailable to the RIS controller. Consequently, the RIS controller configures the reflection coefficient considering no fluctuation exist, yielding the following reflection phase under the optimal phase configuration [13]

$$\varphi_{mn}^{\mathrm{opt}}(t) = \frac{2\pi}{\lambda}\left(\left(\mathbf{d}_{mn}^{\mathrm{loc}}\right)^T \boldsymbol{e}_T^{\mathrm{RIS}}(t) + \left(\mathbf{d}_{mn}^{\mathrm{loc}}\right)^T \boldsymbol{e}_R^{\mathrm{RIS}}(t)\right). \tag{19}$$

Then, we have Theorem 1 for the maximum SNR of the proposed aerial RIS auxiliary system with UAV fluctuation.

Theorem 1: In aerial RIS auxiliary mobile communications, the maximum SNR with the optimal RIS reflection phase configuration in the presence of UAV fluctuation is represented as

$$\eta_{\mathrm{opt}}(t) = M_T M_R \frac{P_T}{\sigma^2} \times \frac{\lambda^2 d_c d_r \cos\beta_{\mathrm{in}}^{\mathrm{RIS}}(t)}{(4\pi)^3\left(\xi_T^{\mathrm{RIS}}(t)\xi_R^{\mathrm{RIS}}(t)\right)^2} \times \frac{\sin^2\left(\frac{\pi}{\lambda}Md_c A_1(t)\right)}{\sin^2\left(\frac{\pi}{\lambda}d_c A_1(t)\right)} \times \frac{\sin^2\left(\frac{\pi}{\lambda}Nd_r A_2(t)\right)}{\sin^2\left(\frac{\pi}{\lambda}d_r A_2(t)\right)}, \tag{20}$$

where $A_1(t)$ and $A_2(t)$ are functions of the UAV fluctuation angles, and their expressions are given in the Appendix.

Proof: See the Appendix for details. ■

Theorem 1 shows that the UAV fluctuation affects the maximum SNR through two aspects, one is the aerial RIS receiving aperture (reflected by $\beta_{\mathrm{in}}^{\mathrm{RIS}}(t)$) and the other is the aerial RIS passive beamforming loss (reflected by the second line in (20)). They constitute the squared-power gain of the aerial RIS [9]. Specifically, the maximum SNR with UAV fluctuation can be regarded as the filtered result of its no-fluctuation counterpart by *sinc* function. The declining trend of the *filtering effect* is controlled by carrier frequency, aerial RIS unit size and number, signal departure and arrival angles, and UAV fluctuation angles. Moreover, when no fluctuation exists, the maximum SNR can be expressed as $\eta_{\mathrm{opt}}(t) = M_T M_R \frac{P_T}{\sigma^2} \times M^2 N^2 \lambda^2 d_c d_r \cos\beta_{\mathrm{in}}^{\mathrm{RIS}}(t)/[(4\pi)^3(\xi_T^{\mathrm{RIS}}(t)\xi_R^{\mathrm{RIS}}(t))^2]$. If the attitude fluctuation angles could be accurately detected, the passive beamforming loss brought by fluctuation can be compensated by the aerial RIS phase controller, yielding the same SNR expression as the no-fluctuation case. In this case, the *filtering effect* can be eliminated and the fluctuation affects the maximum SNR via the receiving aperture only.

IV. Results and Discussions

The parameter settings for the ULAs at the MT and the MR follow those in [15]. Moreover, we set f_c = 28 GHz, P_T = 20 dBm, σ^2 = −80 dBm, ξ_R = 100 m, $\mathbf{p}_{\mathrm{RIS}}(0) = (40, 20, 70)^T$, $Md_c = Nd_r$ = 0.6 m, and $d_c = d_r = \lambda/4$, respectively. The Rayleigh distance of the aerial RIS is smaller than the aerial RIS-terminal distance, thus the far-field assumption holds.

We illustrate the impact of UAV fluctuation on the aerial RIS receiving aperture in Fig. 3. The receiving aperture of the aerial RIS is measured by $MNd_c d_r \cos\beta_{\mathrm{in}}^{\mathrm{RIS}}(t)$, which is affected only by the normal incident angle $\beta_{\mathrm{in}}^{\mathrm{RIS}}(t)$ for fixed-dimension array. Compared with no fluctuation case in [4], Fig. 3 indicates that different fluctuations of the UAV have different impact on the array receiving aperture. Specifically, fluctuation in the yaw direction only has no effect on the normal incident angle and therefore no effect on the receiving aperture. Fluctuation in the pitch and roll directions, on the other hand, have a significant but opposite effect on the normal incident angle. Fig. 3 also implies that with a pitch and/or roll fluctuation, even small angles, the receiving aperture becomes affectable but with slow changing rate by the yaw fluctuation.

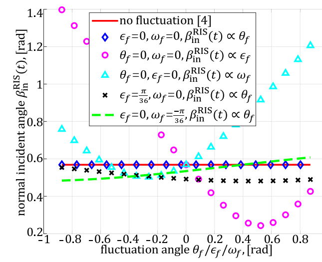

Fig. 3. Impact of UAV fluctuation on the aerial RIS receiving aperture.

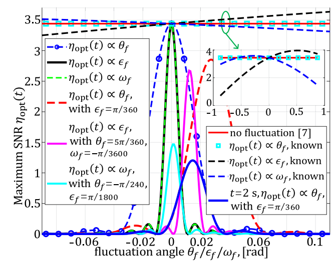

Fig. 4. Impact of UAV fluctuation on the maximum SNR in (20).

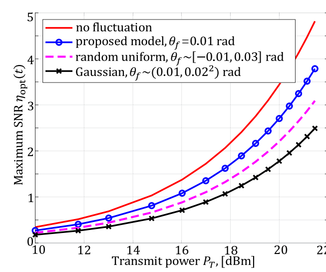

Fig. 5. Impact of different fluctuation models on the maximum SNR.

To explore the theoretical performance gain [9], Fig. 4 shows the maximum SNR of the proposed system versus the UAV attitude fluctuation angles under the optimal reflection phase configuration, where $\theta_f = \epsilon_f = \omega_f = 0$ if not specified. The results show that the fluctuation from all directions will deteriorate the SNR significantly. The SNR declines to an unusable level rapidly with small fluctuation angle, which implies that the UAV fluctuation will result in a *filtering effect* on the SNR as compared to no fluctuation case in [7]. Fig. 4 also shows that two- or three-dimensional fluctuation will shift and scale the SNR curves, thus having more severe effect on the performance as compared to the one-dimensional fluctuation case. When the MT, the aerial RIS, and the MR move to locations (30 m, 10 m, 0), (50 m, 30 m, 70 m), and (130 m, 10 m, 0) at t = 2 s, respectively, the aerial RIS receiving aperture is larger due to smaller $\beta_{\mathrm{in}}^{\mathrm{RIS}}(t)$, but the SNR is deteriorated due to more severe passive beamforming loss. If the UAV attitude fluctuation could be well detected (the curves labeled "known") [11], [12], however, Fig. 4 reveals that the *filtering effect* brought by the fluctuation can be eliminated, indicating that the SNR retains at a favourable level even with large fluctuation angle. In this case, the impact of UAV fluctuation on SNR exhibits the same trend as that on receiving aperture in Fig. 3. This is interpreted by the fact that although the passive beamforming loss caused by fluctuation could be compensated by the aerial RIS phase controller, the impact of fluctuation on $\beta_{\text{in}}^{\text{RIS}}(t)$ and therefore on the receiving aperture still exists. Finally, Fig. 5 compares the impact of different fluctuation models on the maximum SNR, taking the no fluctuation case as the baseline. It reveals that different fluctuation models deteriorate the maximum SNR in different levels, and generally random fluctuations cause more severe performance deterioration.

V. Conclusion

In this letter, we have considered an UAV-mounted RIS auxiliary mmWave mobile communication system with UAV fluctuation. Taking the fluctuation effect into account, a novel aerial RIS assisted mmWave mobile channel model was developed, based on which the performance analysis for the proposed aerial RIS auxiliary system, including the aerial RIS receiving aperture and the maximum SNR, were evaluated in terms of attitude fluctuation. The results showed that the proposed model can effectively capture the effects of UAV fluctuation in the system performance, and fluctuation even with small angles will significantly affect the receiving aperture and the maximum SNR. Moreover, the UAV fluctuation applies a *filtering effect* on the maximum SNR, which could be partially eliminated with accurate UAV attitude detection, and random fluctuation will cause more severe performance deterioration. As future work, we can consider the UAV fluctuation in the 3D location, the closed-form performance metric with random fluctuation models, and the UAV LoS probability model.

Appendix

Under the optimal RIS reflection phase configuration, we have $\chi_{mn}(t) = 1$ and $\varphi_{mn}(t) = \varphi_{mn}^{\text{opt}}(t)$, respectively. Then, the substitution of (19) into (14) yields

$$\Upsilon_{pq}^{\text{opt}}(t) = \Big| \sum_{m=1}^{M} \sum_{n=1}^{N} e^{j\frac{2\pi}{\lambda}\left(\mathbf{d}_{mn}^{\text{loc}} - \mathbf{d}_{mn}\right)^T \left(\boldsymbol{e}_T^{\text{RIS}}(t) + \boldsymbol{e}_R^{\text{RIS}}(t)\right)} \Big|^2. \quad (21)$$

Let $g(t) = \sum_{m=1}^{M}\sum_{n=1}^{N} e^{j\frac{2\pi}{\lambda} g_{mn}(t)}$, then $\Upsilon_{pq}^{\text{opt}}(t) = |g(t)|^2$ and $g_{mn}(t) = (\mathbf{d}_{mn}^{\text{loc}} - \mathbf{d}_{mn})^T(\boldsymbol{e}_T^{\text{RIS}}(t) + \boldsymbol{e}_R^{\text{RIS}}(t))$. According to (4), (7), and (9), we can represent $g_{mn}(t)$ as

$$\begin{aligned}
g_{mn}(t) = {} & k_m d_c \big\{ -\cos\epsilon_f \cos\beta_T^{\text{RIS}}(t) \cos\left(\alpha_T^{\text{RIS}}(t) - \theta_f\right) \\
& - \cos\epsilon_f \cos\beta_R^{\text{RIS}}(t) \cos\left(\alpha_R^{\text{RIS}}(t) - \theta_f\right) \\
& + \sin\epsilon_f \left(\sin\beta_T^{\text{RIS}}(t) + \sin\beta_R^{\text{RIS}}(t)\right) \\
& + \cos\beta_T^{\text{RIS}}(t)\cos\alpha_T^{\text{RIS}}(t) + \cos\beta_R^{\text{RIS}}(t)\cos\alpha_R^{\text{RIS}}(t)\big\} \\
& + k_n d_r \big\{ \sin\epsilon_f \sin\omega_f \cos\beta_T^{\text{RIS}}(t)\cos\left(\alpha_T^{\text{RIS}}(t) - \theta_f\right) \\
& + \sin\epsilon_f \sin\omega_f \cos\beta_R^{\text{RIS}}(t)\cos\left(\alpha_R^{\text{RIS}}(t) - \theta_f\right) \\
& + \cos\omega_f \cos\beta_T^{\text{RIS}}(t)\sin\left(\alpha_T^{\text{RIS}}(t) - \theta_f\right) \\
& + \cos\omega_f \cos\beta_R^{\text{RIS}}(t)\sin\left(\alpha_R^{\text{RIS}}(t) - \theta_f\right) \\
& + \cos\epsilon_f \sin\omega_f \left(\sin\beta_T^{\text{RIS}}(t) + \sin\beta_R^{\text{RIS}}(t)\right) \\
& - \cos\beta_T^{\text{RIS}}(t)\sin\alpha_T^{\text{RIS}}(t) - \cos\beta_R^{\text{RIS}}(t)\sin\alpha_R^{\text{RIS}}(t)\big\} \\
= {} & k_m d_c A_1(t) + k_n d_r A_2(t). \qquad (22)
\end{aligned}$$

Consequently, $g(t)$ can be expressed as

$$\begin{aligned}
g(t) &= \sum_{m=1}^{M}\sum_{n=1}^{N} e^{j\frac{2\pi}{\lambda}\left(k_m d_c A_1(t) + k_n d_r A_2(t)\right)} \\
&= \sum_{m=1}^{M} e^{j\frac{2\pi}{\lambda}\frac{2m-M-1}{2} d_c A_1(t)} \sum_{n=1}^{N} e^{j\frac{2\pi}{\lambda}\frac{2n-N-1}{2} d_r A_2(t)} \\
&\overset{(a)}{=} \frac{\sin\left(\frac{\pi}{\lambda} M d_c A_1(t)\right)}{\sin\left(\frac{\pi}{\lambda} d_c A_1(t)\right)} \times \frac{\sin\left(\frac{\pi}{\lambda} N d_r A_2(t)\right)}{\sin\left(\frac{\pi}{\lambda} d_r A_2(t)\right)}, \qquad (23)
\end{aligned}$$

where (a) exploits the property of geometric sequence.

Then, by substituting (23) into (21) and then into (15), the path power gain under optimal RIS reflection phase configuration with UAV attitude fluctuation can be expressed as

$$\begin{aligned}
\Omega_{\text{RIS}}^{\text{opt}}(t) = {} & \frac{\lambda^2 d_c d_r \cos\beta_{\text{in}}^{\text{RIS}}(t)}{(4\pi)^3\left(\xi_T^{\text{RIS}}(t)\xi_R^{\text{RIS}}(t)\right)^2} \\
& \times \frac{\sin^2\left(\frac{\pi}{\lambda} M d_c A_1(t)\right)}{\sin^2\left(\frac{\pi}{\lambda} d_c A_1(t)\right)} \times \frac{\sin^2\left(\frac{\pi}{\lambda} N d_r A_2(t)\right)}{\sin^2\left(\frac{\pi}{\lambda} d_r A_2(t)\right)}. \qquad (24)
\end{aligned}$$

By substituting (24) into (18), Theorem 1 holds.

References

[1] J. Li et al., "Mobility support for millimeter wave communications: Opportunities and challenges," *IEEE Commun. Surveys Tuts.*, vol. 24, no. 3, pp. 1816–1842, 3rd Quart., 2022.

[2] B. Xiong, Z. Zhang, and H. Jiang, "Reconfigurable intelligent surface for mmWave mobile communications: What if LoS path exists?," *IEEE Wireless Commun. Lett.*, vol. 12, no. 2, pp. 247–251, Feb. 2023.

[3] C. You, Z. Kang, Y. Zeng, and R. Zhang, "Enabling smart reflection in integrated air-ground wireless network: IRS meets UAV," *IEEE Wireless Commun.*, vol. 28, no. 6, pp. 138–144, Dec. 2021.

[4] X. Tang, D. Wang, R. Zhang, Z. Chu, and Z. Han, "Jamming mitigation via aerial reconfigurable intelligent surface: Passive beamforming and deployment optimization," *IEEE Trans. Veh. Technol.*, vol. 70, no. 6, pp. 6232–6237, Jun. 2021.

[5] H. Zhang and L. Hanzo, "Aerial reconfigurable intelligent surface assisted maritime wireless communications," in *Proc. IEEE WCSP*, Nanjing, China, 2022, pp. 916–921.

[6] L. Ge, H. Zhang, J.-B. Wang, and G. Y. Li, "Reconfigurable wireless relaying with multi-UAV-carried intelligent reflecting surfaces," *IEEE Trans. Veh. Technol.*, vol. 72, no. 4, pp. 4932–4947, Apr. 2023.

[7] M.-H. T. Nguyen, E. Garcia-Palacios, T. Do-Duy, O. A. Dobre, and T. Q. Duong, "UAV-aided aerial reconfigurable intelligent surface communications with massive MIMO system," *IEEE Trans. Cogn. Commun. Netw.*, vol. 8, no. 4, pp. 1828–1838, Dec. 2022.

[8] W. Wang and W. Zhang, "Jittering effects analysis and beam training design for UAV millimeter wave communications," *IEEE Trans. Wireless Commun.*, vol. 21, no. 5, pp. 3131–3146, May 2022.

[9] Q. Wu and R. Zhang, "Intelligent reflecting surface enhanced wireless network via joint active and passive beamforming," *IEEE Trans. Wireless Commun.*, vol. 18, no. 11, pp. 5394–5409, Nov. 2019.

[10] B. Xiong et al., "A statistical MIMO channel model for reconfigurable intelligent surface assisted wireless communications," *IEEE Trans. Commun.*, vol. 70, no. 2, pp. 1360–1375, Feb. 2022.

[11] J. Zhang, L. Ren, H. Deng, M. Ma, X. Zhong, and P. Wen, "Measurement of unmanned aerial vehicle attitude angles based on a single captured image," *Sensors*, vol. 18, no. 8, p. 2655, Aug. 2018.

[12] P. Wang, W. Mei, J. Fang, and R. Zhang, "Target-mounted intelligent reflecting surface for joint location and orientation estimation," *IEEE J. Sel. Areas Commun.*, vol. 41, no. 12, pp. 3768–3782, Dec. 2023.

[13] B. Xiong, Z. Zhang, H. Jiang, J. Zhang, L. Wu, and J. Dang, "A 3D non-stationary MIMO channel model for reconfigurable intelligent surface auxiliary UAV-to-ground mmWave communications," *IEEE Trans. Wireless Commun.*, vol. 21, no. 7, pp. 5658–5672, Jul. 2022.

[14] X. Li, H. Lu, Y. Zeng, S. Jin, and R. Zhang, "Near-field modeling and performance analysis of modular extremely large-scale array communications," *IEEE Commun. Lett.*, vol. 26, no. 7, pp. 1529–1533, Jul. 2022.

[15] H. Jiang, B. Xiong, H. Zhang, and E. Basar, "Hybrid far- and near-field modeling for reconfigurable intelligent surface assisted V2V channels: A sub-array partition based approach," *IEEE Trans. Wireless Commun.*, vol. 22, no. 11, pp. 8290–8303, Nov. 2023.